Rigorous Full-Wave Space-Domain Solution for Dispersive Microstrip Lines

NIELS FACHÉ AND DANIËL DE ZUTTER

Abstract—**The eigenmode problem for the open microstrip line is analyzed in the space domain starting from the calculation of a dyadic Green's function in the spectral domain. The transverse and the longitudinal current are discretized using the method of moments. A point-matching technique is used to impose the boundary condition, i.e., zero tangential electric field, on the strip. The edge conditions at the end points of the strip are explicitly incorporated and special care is taken to accurately retain the static behavior of the fields on and near the strip. Special attention is devoted to the variation of the current distribution as a function of frequency.**

I. Introduction

THE DISPERSION characteristics and the (lowest) eigenmode(s) propagating along an open microstrip line have been analyzed by a large number of authors. We refer the reader to [1]–[10] for a review of the various approaches and results. The spectral-domain approach proposed in [1] and [2] was recently applied by Kobayashi and Ando [6] to determine the frequency dependence of the effective dielectric constant starting from a closed-form expression for the transverse and the longitudinal current distribution on the strip. These expressions take the edge conditions into account.

In the spectral-domain approach proposed by [1], the boundary conditions on the strip, i.e., the vanishing tangential electric and normal magnetic field, are only satisfied at a single point at the center of the strip. In more recent publications using the spectral-domain approach [2]–[10], either a more accurate closed-form representation of the current or a representation of the current using a larger number of basis functions is introduced. In these cases the boundary conditions are imposed in some global sense.

In the present paper a full-wave solution is proposed in the space domain starting from the calculation of a dyadic Green's function in the spectral domain. Both the transverse and the longitudinal current are discretized using the method of moments in such a way that the edge conditions are satisfied. The boundary conditions on the strip are no longer imposed in a global sense but at a number of points equally spaced along the strip. In addition, by explicitly satisfying the boundary conditions at the end points of the strip, the static behavior of the fields on and near the strip is accurately retained in our approach. As we do not start from a closed-form expression of the current on the strip, as in [6], it becomes possible to examine the influence of the frequency on the current distribution. Another considerable advantage of the proposed method is the fact that it can be extended to study the coupling between two or more microstrip lines. As the dyadic Green's function is found in the spectral domain, the method is suited to coupling between lines in the same horizontal plane, as well as to lines at different depths in a multilayered structure. In the latter case it is essential to include enough degrees of freedom in the representation of the current distribution.

Manuscript received June 22, 1987; revised October 20, 1987. This work was supported in part by a grant from the Instituut tot Aanmoediging van het Wetenschappelijk Onderzoek in Nijverheid en Landbouw.

The authors are with the Laboratory of Electromagnetism and Acoustics, University of Ghent, 9000 Ghent, Belgium.

IEEE Log Number 8719200.

II. General Formulation

The structure under consideration is shown in Fig. 1. The ground plane at $z = 0$ is perfectly conducting and the microstrip substrate (medium 1) with thickness d consists of a lossless, nonmagnetic material with relative permittivity ϵ_r. The strip is infinitely thin and perfectly conducting, with width $2w$ $(-w \leqslant y \leqslant +w)$. The medium above the strip is air (medium 2).

As we want to determine the lowest eigenmode propagating along the microstrip line, all field components depend upon x through the common phase factor $\exp(-j\beta x)$, where β represents the propagation constant of the eigenmode. The time dependence $\exp(j\omega t)$ is suppressed. For the calculation of the electromagnetic fields excited by the eigenmode, we start from the surface current density on the strip:

$$\begin{aligned} j_x(x, y) &= J_x(y)e^{-j\beta x} \\ j_y(x, y) &= J_y(y)e^{-j\beta x} \end{aligned} \qquad -w \leqslant y \leqslant +w. \tag{1}$$

The electric field generated by these surface currents everywhere in space can be found with the help of a suitable Green's dyadic $\bar{\bar{G}}$:

$$\boldsymbol{E}(y, z) = \int_{-w}^{w} \bar{\bar{G}}(y, z; y', z' = d, \beta) \cdot \boldsymbol{J}(y')\, dy'. \tag{2}$$

The actual electric field is $\boldsymbol{e} = \exp(-j\beta x)\bar{\boldsymbol{E}}$. The coordinates z and y are the coordinates of an observation point outside the strip and y' stands for the coordinate of a variable integration point along the strip. As the surface current density $\boldsymbol{J}$ is as yet unknown, $\boldsymbol{J}$ can be found by

0018-9480/88/0400-0731$01.00

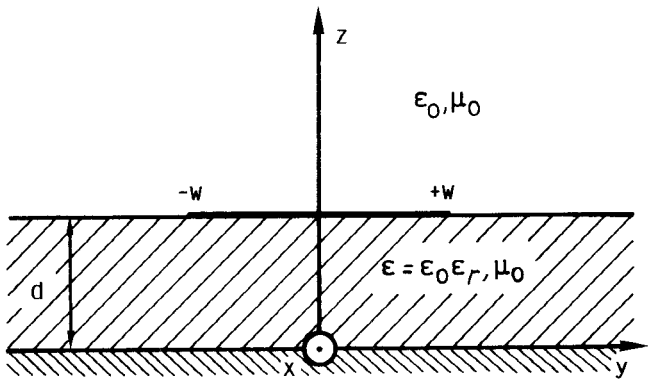

Fig. 1. Perfectly conducting microstrip line on a dielectric substrate.

expressing the fact that the tangential component of the electric field $\boldsymbol{E}$ given by (2) must vanish on the strip itself. This leads to the following integral equation:

$$\lim_{z \to d} \int_{-w}^{w} \overline{\overline{G}}_t(y, z; y', z' = d, \beta) \cdot \boldsymbol{J}(y')\, dy' = 0. \quad (3)$$

The observation point is now restricted to the strip, where $z \to d$ and $-w \leqslant y \leqslant +w$. $\overline{\overline{G}}_t$ represents this part of $\overline{\overline{G}}$ which yields the tangential x and y components of $\boldsymbol{E}$. The above integral equation constitutes an eigenvalue problem. The propagation constant β is the eigenvalue of the problem and the current on the strip forms the associated eigenvector. The kernel $\overline{\overline{G}}_t$ depends upon the eigenvalue β. As will be shown below, it is essential to retain the limit $z \to d$. A mere interchange of this limit with the integration over y' is not always allowed.

III. Discretization of the Surface Current

For the solution of (3) we use the method of moments combined with a point-matching technique. The strip is divided into N identical intervals with width Δ (see Fig. 2). The modeling in the intervals 2 to $N-1$ is based on a superposition of elementary triangular functions which extend over two intervals. This leads to a piecewise-linear representation of both the longitudinal and the transverse current. In the outermost intervals 1 and N, our representation explicitly accounts for the behavior of the electromagnetic fields near the edges. This behavior has been analyzed by Meixner [11] and imposes the following form for the longitudinal current:

$$J_x = A\tau^{-1/2} + B\tau^{1/2} + C\tau^{3/2} + O(\tau^{5/2}) \quad (4)$$

where τ represents the distance to the edge. This component of the current becomes infinite at the edge. The transversal component remains finite:

$$J_y = B'\tau^{1/2} + C'\tau^{3/2} + O(\tau^{5/2}). \quad (5)$$

In our discretization of the current we restrict the series (4) to the first three terms and the series (5) to the first two terms. To ensure continuity of the current along the strip and to incorporate the behavior near the edges, the current representation in the intervals 1 and 2 is supplemented by the superposition of the modified triangular functions

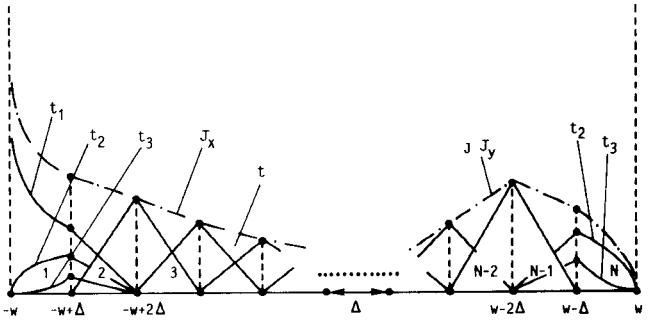

Fig. 2. Longitudinal current J_x and transversal current jJ_y as a superposition of elementary basis functions.

$t_1(y)$, $t_2(y)$, and $t_3(y)$ for the longitudinal component and $t_2(y)$ and $t_3(y)$ for the transverse component:

$$t_1(\tau) = (\Delta/\tau)^{1/2}$$
$$t_2(\tau) = (\tau/\Delta)^{1/2}$$
$$t_3(\tau) = (\tau/\Delta)^{3/2} \quad (6)$$

for $0 < \tau < \Delta$ and

$$t_1(\tau) = t_2(\tau) = t_3(\tau) = (2\Delta - \tau)/\Delta$$

for $\Delta < \tau < 2\Delta$, where $\tau = w - |y|$ at both edges.

An analogous approach is implemented near the other edge. Fig. 2 shows the basis functions and their superposition for the longitudinal current $J_x(y)$ at the left-hand part of the figure and for the transverse current $J_y(y)$ at the right hand. As shown below, both components are in quadrature. The total number of scalar unknowns introduced in the way outlined above is $2N+4$. To determine these unknowns we require the integral equation (3) to be satisfied in $N+2$ points. These $N+2$ sample points are chosen to be in the center of each interval and at the edges of the strip.

The above approach allows us to reduce the original integral equation to the discrete matrix problem:

$$[A][J] = [0]. \quad (7)$$

The square matrix $[A]$ has $(2N+4)\times(2N+4)$ elements and the column vector $[J]$ contains the unknowns which model the surface current. The eigenmode calculation is now reduced to the determination of the eigenvalue β for which $\det[A]$ becomes zero. The corresponding eigenvector $[J]$ is found by satisfying the $2N+4$ linear equations in (7) using a least-squares technique.

IV. Green's Dyadic in the Fourier Domain

As a first step we introduce the Fourier transformation of all fields with respect to the y coordinate. The Fourier transformation and its inverse are defined as follows:

$$F(k_y) = (1/2\pi) \int_{-\infty}^{+\infty} f(y) \exp(jk_y y)\, dy$$
$$f(y) = \int_{-\infty}^{+\infty} F(k_y) \exp(-jk_y y)\, dk_y. \quad (8)$$

As there is no danger for confusion, we have not introduced a special symbol to indicate the Fourier transforma-

tion. A function and its transformation are only distinguished by their arguments. It is easy to see from Maxwell's equations that the transformed fields in medium 1 and 2 satisfy

$$\frac{d^2\boldsymbol{E}}{dz^2} - \Gamma^2\boldsymbol{E} = 0$$
$$\frac{d^2\boldsymbol{H}}{dz^2} - \Gamma^2\boldsymbol{H} = 0 \tag{9}$$

with $\Gamma^2 = \beta^2 + k_y^2 - k_0^2 N^2$. Here $k_0 = \omega/c$ is the wavenumber, $N = \sqrt{\epsilon_r}$ for medium 1, and $N = 1$ for medium 2. Γ itself is defined as the root of Γ^2 with nonnegative real or imaginary part. The general solution of (9) is given by

$$\boldsymbol{E}(z, k_y, \beta) = \boldsymbol{A}\exp(-\Gamma z) + \boldsymbol{B}\exp(\Gamma z)$$
$$\boldsymbol{H}(z, k_y, \beta) = \boldsymbol{K}\exp(-\Gamma z) + \boldsymbol{L}\exp(\Gamma z). \tag{10}$$

The vectors $\boldsymbol{K}$ and $\boldsymbol{L}$ are not independent of $\boldsymbol{A}$ and $\boldsymbol{B}$. The relation between them will be established below.

As a second and essential step we introduce the projection of every vector on three orthogonal directions. An arbitrary vector $\boldsymbol{W}$ is characterized by the three numbers W_z, W', and W'' as follows:

$$\boldsymbol{W} = W_z\boldsymbol{u}_z + [W'\boldsymbol{k} + W''(\boldsymbol{u}_z \times \boldsymbol{k})]/(\beta^2 + k_y^2)$$
$$\boldsymbol{k} = \beta\boldsymbol{u}_x + k_y\boldsymbol{u}_y \quad \text{and} \quad k^2 = \beta^2 + k_y^2. \tag{11}$$

It is clear that the corresponding values E', E'', E_z, H', H'', and H_z are of the form (10) but with the vectors replaced by scalars. With the notation introduced above, Maxwell's divergence equations reduce to $dE_z/dz = JE'$ and to $dH_z/dz = jH'$. The rotor equations projected on the z axis yield the relations $E'' = \omega\mu_0 H_z$ and $H'' = -\omega\epsilon_0\epsilon_r E_z$. Taking the above results and considerations into account, we finally arrive at the following representation of the fields in each layer:

$$E'(z, k_y, \beta) = A'\exp(-\Gamma z) + B'\exp(\Gamma z)$$
$$H''(z, k_y, \beta) = (j\omega\epsilon_0\epsilon_r/\Gamma)[A'\exp(-\Gamma z) - B'\exp(\Gamma z)]$$
$$E_z(z, k_y, \beta) = (-j/\Gamma)[A'\exp(-\Gamma z) - B'\exp(\Gamma z)] \tag{12}$$

and

$$E''(z, k_y, \beta) = A''\exp(-\Gamma z) + B''\exp(\Gamma z)$$
$$H'(z, k_y, \beta) = [\Gamma/(-j\omega\mu_0)] \cdot [A''\exp(-\Gamma z) - B''\exp(\Gamma z)]$$
$$H_z(z, k_y, \beta) = (1/\omega\mu_0)[A''\exp(-\Gamma z) + B''\exp(\Gamma z)]. \tag{13}$$

As shown by (12) and (13), this representation of the fields falls apart into two sets of decoupled equations: one set for E', H'', and E_z and a second set for E'', H', and H_z. The first set is a TM mode as the z component of the magnetic field is zero. The second set is a TE mode. The couples (E', H'') and (E'', H') can be used to define equivalent voltage and current across a transmission line.

The constants A', B' and A'', B'' must be determined by applying the boundary conditions between the layers of the medium. The continuity of the tangential electric field between substrate and air leads to

$$\begin{aligned} E_1' - E_2' &= 0 \\ E_1'' - E_2'' &= 0 \end{aligned} \quad \text{for } z = d. \tag{14}$$

The tangential magnetic field exhibits a jump at the strip. The appropriate boundary condition is

$$\begin{aligned} H_1' - H_2' &= -J''(k_y) \\ H_1'' - H_2'' &= +J'(k_y) \end{aligned} \quad \text{for } z = d \tag{15}$$

where $\boldsymbol{J}(k_y) = J_x(k_y)\boldsymbol{u}_x + J_y(k_y)\boldsymbol{u}_y$ represents the Fourier-transformed surface current density $\boldsymbol{J}(y)$ (3). Additional boundary conditions are given by the fact that E' and E'' are zero at the perfectly conducting ground plane, i.e., for $z = 0$; hence $A_1' + B_1' = 0$ and $A_1'' + B_1'' = 0$. Finally, in medium 2, only outgoing waves can exist. This implies $B_2' = 0$ and $B_2'' = 0$. After some manipulations we arrive at the following result for $\overline{\overline{G}}_t(k_y, z)$ (3) for an arbitrarily oriented surface current element located at $y = y'$:

$$G_{txx} = (a\beta^2 + bk_y^2)\exp[-\Gamma_2(z-d)]\exp(jk_y y')/k^2$$
$$G_{txy} = G_{tyx} = (a-b)k_y\beta\exp[-\Gamma_2(z-d)]\exp(jk_y y')/k^2$$
$$G_{tyy} = (ak_y^2 + b\beta^2)\exp[-\Gamma_2(z-d)]\exp(jk_y y')/k^2 \tag{16}$$

with

$$a = \frac{-\Gamma_1\Gamma_2\sinh(\Gamma_1 d)}{j\omega\epsilon_0[\Gamma_1\sinh(\Gamma_1 d) + \epsilon_r\Gamma_2\cosh(\Gamma_1 d)]}$$
$$b = \frac{-j\omega\mu_0\sinh(\Gamma_1 d)}{[\Gamma_2\sinh(\Gamma_1 d) + \Gamma_1\cosh(\Gamma_1 d)]}. \tag{17}$$

Γ_1 and Γ_2 are defined in (9). Strictly speaking, (16) and (17) are only valid for $z > d$. For the integral equation (3) we actually need the limit $z \to d$ in (16).

V. Green's Dyadic in the Space Domain

To find $\overline{\overline{G}}_t(y, z)$ in the space domain, the inverse Fourier transformations of the elements of $\overline{\overline{G}}_t(k_y, z)$ in (16) must be determined. This calculation reduces to the determination of six Fourier integrals which can be taken together into two classes:

$$(j/\omega\epsilon_0)\int_{-\infty}^{+\infty} \frac{\Gamma_1\Gamma_2 k_y' \exp[-\Gamma_2(z-d) - jk_y\delta]}{[\Gamma_1 + \epsilon_r\Gamma_2\coth(\Gamma_1 d)](\beta^2 + k_y^2)}\,dk_y \tag{18}$$

and

$$-j\omega\mu_0\int_{-\infty}^{+\infty} \frac{k_y' \exp[-\Gamma_2(z-d) - jk_y\delta]}{[\Gamma_2 + \Gamma_1\coth(\Gamma_1 d)](\beta^2 + k_y^2)}\,dk_y. \tag{19}$$

The notation $\delta = y - y'$ stands for the distance between the observation point and the source point on the strip.

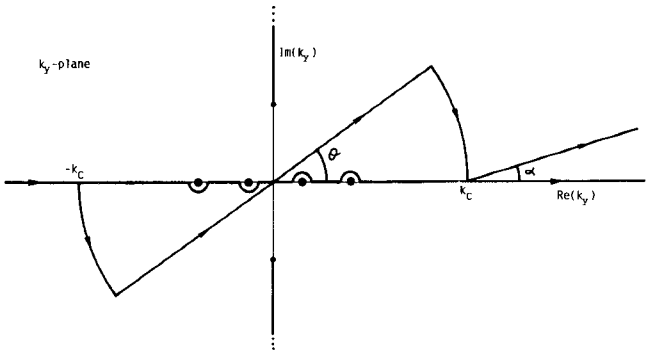

Fig. 3. Integration path, singularities, and branch cuts in the complex k_y plane.

The superscript i, indicating a power of k_y, takes the values 0, 1, and 2. From (16) and (17) it can be seen that $G_{txx}(k_y)$ and $G_{tyy}(k_y)$ are even with respect to k_y while $G_{txy}(k_y) = G_{tyx}(k_y)$ is odd and that the coefficients a and b (17) take an imaginary value. Consequently $G_{txx}(y-y')$ and $G_{tyy}(y-y')$ are even with respect to δ, and $G_{txy}(y-y')$ is odd, while $J_x(y)$ will be even with respect to y and J_y will be odd. Moreover, $J_x(y)$ and $J_y(y)$ are in quadrature.

At this point it is justified to interchange the limit $z \to d$ with the integration over y' in (3) on the explicit condition that the above integrals (18) and (19) remain bounded for $z = d$. This is not the case when the source and the observation point coincide, i.e., for $\delta = 0$ or $y = y'$. The approach followed in that particular case, i.e., for the self-patch calculations, is discussed in the next section. In the present section we now assume $z = d$ in (16), (18), and (19).

The integrals (18) and (19) for $i = 1,2$ can be derived from those for $i = 0$ by taking, respectively, the first and second derivative with respect to δ. Hence, the discussion will be restricted to the case $i = 0$. Fig. 3 shows the integration path along the real k_y axis. The poles are excluded in such a way as to satisfy the appropriate causality conditions [12]. As indicated on Fig. 3, the integration path from $-\infty$ to $+\infty$ is divided into three intervals: $[-\infty, -k_c]$, $[-k_c, +k_c]$, and $[+k_c, +\infty]$. The value of k_c is chosen such that Γ_1 and Γ_2 can be approximated by $|k_y|$ while $\beta^2 + k_y^2$ can be replaced by k_y^2 in the first and third intervals. This implies that the contributions to (18) and (19) coming from $[-\infty, -k_c]$ and from $[+k_c, \infty]$ can be taken together. The contribution to (18) for $i = 0$ and $z = d$ is

$$\frac{-4j\epsilon_r}{\omega\epsilon_0(1+\epsilon_r)^2}\,\mathrm{Re}\left[\int_{k_c}^{+\infty}\frac{\exp(-2k_y d - jk_y\delta)}{\left[1+K\exp(-2k_y d)\right]k_y}\,dk_y\right] + \frac{2j}{\omega\epsilon_0(1+\epsilon_r)}\int_{k_c}^{+\infty}\frac{\cos(k_y\delta)}{k_y}\,dk_y \tag{20}$$

where $K = (\epsilon_r - 1)/(\epsilon_r + 1)$. The contribution to (19) for $i = 0$ and $z = d$ becomes

$$-j\omega\mu_0\int_{k_c}^{+\infty}\frac{\cos(k_y\delta)}{k_y^3}\left[1-\exp(-2k_y d)\right]dk_y. \tag{21}$$

A typical value for k_c is $10\times k_0\times\epsilon_r$. The integrations in (20) and (21) no longer depend upon β. Hence, in spite of the iterative method used to determine the value of β which satisfies $\det[A] = 0$ in (7), the integrations involved in that iterative process stemming from (20) and (21) must be performed only once. This is a considerable advantage of the proposed method. The contribution (21) can be found analytically. The result is

$$\begin{aligned}&-(j\omega\mu_0/2k_c^2)\Big(\left[\cos(k_c\delta) - k_c\delta\sin(k_c\delta)\right.\\&\quad\left.+(k_c\delta)^2\,\mathrm{ci}(|k_c\delta|)\right]\\&\quad-\left[\cos(k_c\delta) - 2k_c d\cos(k_c\delta)\right.\\&\quad\left.-k_c\delta\sin(k_c\delta)\right]\exp(-2k_c d)\Big)\\&\quad+j\omega\mu_0/2\,\mathrm{Re}\left[(-2d+j\delta)^2E_1(2k_c d - jk_c\delta)\right]\end{aligned} \tag{22}$$

where ci denotes the cosine integral and E_1 the exponential integral [13]. The contribution (20) has been written as the sum of two integrals in such a way that the second integral contains the dominant behavior for $y \to y'$ ($\delta \to 0$). This second integral can be found analytically:

$$-j2\,\mathrm{ci}(|k_c\delta|)/\left[\omega\epsilon_0(1+\epsilon_r)\right]. \tag{23}$$

Consequently, the first class of integrals (18) has a logarithmic singularity $\ln|y-y'|$ for $i = 0$. This implies a $1/|y-y'|$ singularity for $i = 1$ and a $1/|y-y'|^2$ singularity for $i = 2$. The second class (19) only exhibits a logarithmic singularity for $i = 2$.

The first integral in (20) must be calculated numerically. Because of strong oscillation of the integrand, the integration path is deformed to a suitable straight line in the complex k_y plane as shown on the right of Fig. 3:

$$k_y = \tau + j(\tau - k_c)\delta/(2d), \qquad k_c < \tau < \infty. \tag{24}$$

The angle α on Fig. 3 is defined by $\tan(\alpha) = \delta/2d$. The path is chosen such that the phase factor $\exp(-2k_y d + jk_y\delta)$ in the integrand decays exponentially along the path, reducing most of the oscillation of that integrand along the original path. The actual numerical integration is based on the Gauss–Laguerre quadrature.

Finally, we have to deal with the integrals over the interval $[-k_c, +k_c]$. Due to the resonant modes of the structure, the integrands for the first class of integrals (18) exhibit a finite number of poles in this interval. As medium 1 and medium 2 are both nonmagnetic, this is not the case for the second class (19). The poles are indicated on Fig. 3 together with the branch cuts necessary to define the values of Γ_1 and Γ_2. To avoid the singularities, the original integration path $[-k_c, +k_c]$ along the real k_y axis is replaced by a new one consisting of a straight line through the origin together with two arcs (see Fig. 3). The angle θ, which in principle takes an arbitrary value, is chosen such that the amplitude variation of the integrand remains small enough to ensure the accuracy of the numerical integration. The integration from $-k_c$ to $+k_c$ for the second class (19) takes place along the real axis. In both cases

simple Gaussian quadrature is used except when $c/(2fw\sqrt{\epsilon_r}) < 1$ (c: velocity of light in vacuum, f: frequency). In the latter case a Filon quadrature is more appropriate.

For sufficiently low frequencies the exponential factor $\exp(-jk_y\delta)$ in the integrals over $[-k_c, +k_c]$ can be expanded in a power series in $k_y\delta$. As a consequence of this expansion the integrals we are searching for can be approximated by polynomials in δ, the coefficients of which are integrals which still depend on β but not on δ. As we need these integrals for a whole range of δ values, this approach considerably reduces the calculation effort. In the example considered in the section on numerical results, the series expansion approach yields correct results up to 100 MHz.

VI. Self-Patch Contribution

If we consider a specific point-matching point y, the self-patch contribution to (3) is the contribution coming from the integration over the interval Δ to which y belongs. In that particular case interchanging the limit $z \to d$ in (3) with the integration over y' is not allowed as it leads to divergent results. At this point we will not go into the details of the calculations. The approach that must be followed will be illustrated by determining the self-patch contributions for the point-matching point y placed at one of the edges of the strip. We start from (18) and (19) but retain the limit $z \to d$ in the integration over $[-\infty, -k_c]$ and $[+k_c, \infty]$. One can show that this is not necessary for the integration over $[-k_c, +k_c]$ as the integrand has a regular behavior for $z = d$. Hence, this part of the contribution can be treated as explained in the preceding section. Self-patch contributions to the matrix $[A]$ in (7) for $y = -w$ and coming from the integration of $G_{txy}J_y$ and of $G_{txx}J_x$ in (3) remain finite if $z \to d$. We focus our attention on those contributions which become infinite. The nonregular behavior of the integral in the left-hand member of (3) for $z \to d$ and for $y = -w$ comes from

$$\lim_{z\to d}\int_{-w}^{-w+\Delta}\left[G_{tyx}(y=-w,z;\ y',z'=d,\beta)J_x(y') + G_{tyy}(y=-w,z;\ y',z'=d,\beta)J_y(y')\right]dy'. \quad (25)$$

The current J_x is built up as a superposition of functions proportional to t_1, t_2, and t_3 (6), and J_y is built up as a superposition of functions proportional to t_2 and t_3. A detailed analysis shows that the nonregularity comes only from t_1 in the case of J_x and from t_2 in the case of J_y. From (16) it can be seen that G_{tyx} and G_{tyy} consist of two parts: a first part proportional to the coefficient a (17) being the TM part, and a second part proportional to the coefficient b (17) being the TE part. Only the TM part is responsible for the nonregularity in (25). This is due to the fact that the TM part of G_{tyx} becomes a nonzero constant for $k_y \to \infty$ and that the TM part of G_{tyy} is proportional to k_y for large values of k_y, while the TE part vanishes as $1/k_y^2$ in the case of G_{tyx} and as $1/k_y^3$ in the case of G_{tyy}. In the sequel we disregard the TE contributions. The first term in (25) for $J_x = At_1$ and for the TM part of G_{tyx} leads to

$$\lim_{z\to d}\int_0^{\Delta}A(y')^{-1/2}dy'\int_{k_c}^{+\infty}-j\beta\kappa\sin(k_yy')\cdot\exp(-k_y|z-d|)\,dk_y = -j\kappa\beta A\Big(\lim_{z\to d}\left[\pi 2^{-1/2}|z-d|^{-1/2}\right] - 2\cos(k_c\Delta)(\Delta)^{-1/2} - 2(2\pi k_c)^{1/2}S(k_c\Delta)\Big) \quad (26)$$

while the second one for $J_y = B't_2$ and for the TM part of G_{tyy} gives

$$\lim_{z\to d}\int_0^{\Delta}B'(y')^{1/2}dy'\int_{k_c}^{+\infty}(-)\kappa k_y\cos(k_yy')\cdot\exp(-k_y|z-d|)\,dk_y = -\kappa B'\Big(\lim_{z\to d}\left[-\pi 2^{-3/2}|z-d|^{-1/2}\right] + 2\cos(k_c\Delta)(\Delta)^{-1/2} + (2\pi k_c)^{1/2}S(k_c\Delta)\Big). \quad (27)$$

In both (26) and (27) $S(k_c\Delta)$ represents the Fresnel sine integral of argument $k_c\Delta$ [13]. The coefficients κ in (26) and (27) is given by $\kappa = 2/[j\omega\epsilon_0(1+\epsilon_r)]$. The coefficient A in (26) is the same as in (4). As $\omega \to 0$, A remains constant and the ratio β/ω in $\beta\kappa$ takes a constant nonzero value. On the other hand, B' in (27) is the same as in (5). As $\omega \to 0$, B' must also vanish because no transversal current is found on the strip for $\omega = 0$. However, the product $\kappa B'$ in (27) takes a constant nonzero value for $\omega \to 0$. The above considerations show that the self-patch contributions in (26) and (27) still differ from zero for $\omega = 0$ and that their correct evaluation leads to the correct static behavior of the lowest eigenmode and associated eigenvalue β. Although the tangential electric field is zero everywhere on the strip, i.e., for $z = d$, this is not the case just below or just above the strip. Both the longitudinal current and the transversal current give rise to an electric field component which in fact becomes infinite just above the edges of the strip as required by Meixner's edge condition. For the actual self-patch contributions the terms in $|z-d|^{-1/2}$ in (26) and (27) must be dropped. These nonregular parts correspond to the static field in the neighborhood of the edge of the strip. The remaining contributions are regular.

VII. Numerical Results

The main interest of this paper lies in the presentation of a new approach for the solution of the eigenproblem for the microstrip line. Consequently, we restrict the numerical results presented in this section to a typical configuration which can be found in several publications [1]–[3], [6]. In this configuration the relevant parameters take the values $2w = 3.04$ mm, $d = 3.17$ mm, and $\epsilon_r = 11.7$. Fig. 4 shows the value of the effective dielectric constant $(\epsilon_r)_{\text{eff}} = (\beta/k)^2$ as a function of frequency $f = \omega/2\pi$ and this up to 15 GHz. We have compared this result with the one

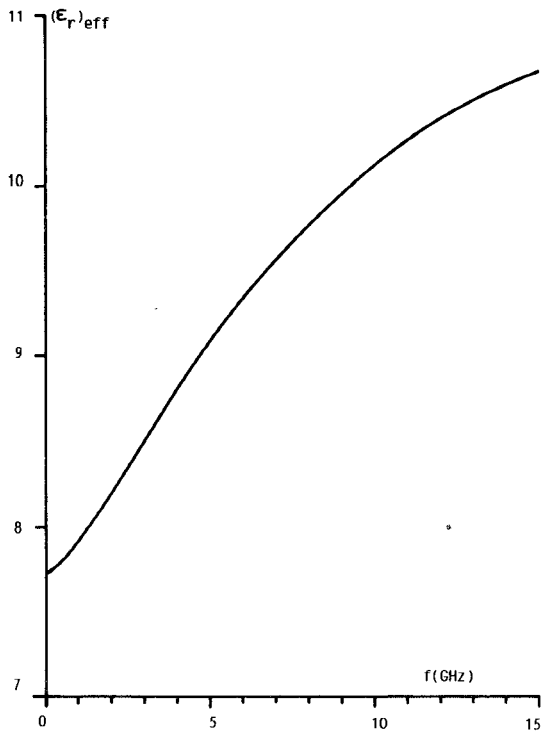

Fig. 4. Effective dielectric constant as a function of frequency for the configuration of Fig. 1 with $2w = 3.04$ mm, $d = 3.17$ mm, and $\epsilon_r = 11.7$.

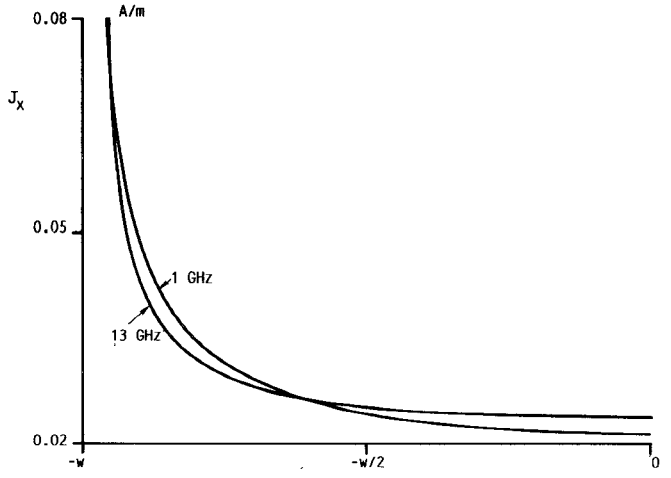

Fig. 5. Longitudinal current J_x at 1 GHz and 13 GHz, relevant to the example of Fig. 1.

obtained by Kobayashi *et al.* [6] with the spectral-domain method based on an *a priori* form of the longitudinal and the transverse current. Both results differ less than 1 percent up to 10 GHz, which is the highest frequency considered in [6]. The reader is referred to the paper by Kobayashi *et al.* for a detailed comparison of their results with the ones obtained by other authors. The numerical results shown in Fig. 4 (with an accuracy of 0.1 percent) were obtained by a division of the strip into 10 intervals.

The longitudinal current and the transversal current on the strip are shown in Figs. 5 and 6, respectively. As the longitudinal current is symmetric with respect to the center of the strip and as the transversal current is antisymmetric,

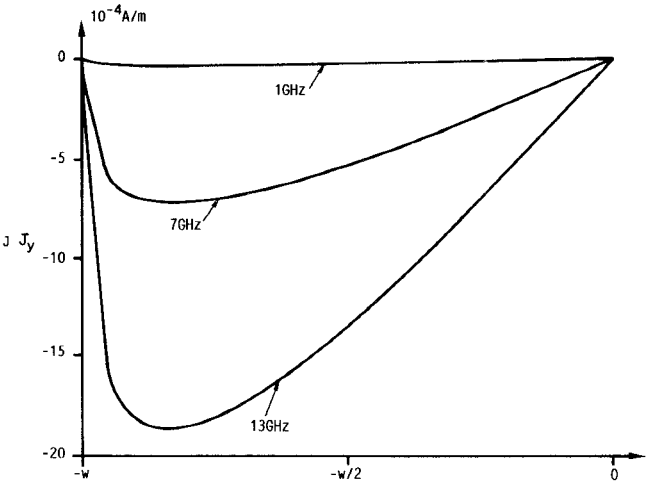

Fig. 6. Transversal current jJ_y at 1 GHz, 7 GHz, and 13 GHz relevant to the example of Fig. 1.

we display only the results for the left half of the strip. The transverse current increases with increasing frequency. However, at 13 GHz it still remains two orders of magnitude smaller than the longitudinal current. J_x and J_y are in quadrature. As the amplitude of the transverse current changes more rapidly as a function of frequency than the longitudinal current, J_y is plotted for three different frequencies while J_x is depicted for only two frequencies. The total longitudinal current, i.e., the integral of J_x over the width of the strip, is kept constant for each frequency. The result for 13 GHz in Fig. 5 shows a kind of skin effect. As the frequency increases, the longitudinal current tends to be constant over a larger portion of the strip, as would be the case for an infinite strip, and the singular behavior becomes more and more restricted to the immediate neighborhood of the edges. The results of Figs. 5 and 6 clearly exhibit the ability of our method to allow for a variation of the current profile as a function of frequency.

The dispersion characteristic of Fig. 4 changes only marginally if the number of divisions on the strip is increased beyond 10. For the current profiles, however, at least 30 divisions are necessary to obtain a converging result.

VIII. Conclusions

We have shown that a rigorous full-wave space-domain solution for a dispersive microstrip line offers an alternative to the spectral-domain method. This solution also starts from the spectral domain for the calculation of an appropriate dyadic Green's function. Explicit inversion of this Green's dyadic leads to the Green's dyadic in the space domain. This dyadic is used as the kernel of an integral equation for the vanishing tangential electric field on the strip. The integral equation itself was solved using the method of moments and a point-matching technique. The analysis of the problem shows that it is possible to incorporate Meixner's edge conditions at the end points of the strip. Moreover, it is shown that by incorporating these edge conditions and by explicitly satisfying the integral

equation at the end points, the correct low-frequency and static behavior of all field quantities is ensured. A considerable advantage of the method lies in the fact that no prior knowledge of the current density on the strip is necessary. This makes the method suitable for analyzing multistrip configurations. The analysis and numerical data concerning multilayered and/or multistrip configurations will be presented in a forthcoming paper. The numerical results given in this paper illustrate the capability of the method to calculate the dispersion characteristics of a single microstrip line up to very high frequencies and to study the change in the surface current density as a function of frequency.

REFERENCES

[1] E. J. Denlinger, "A frequency dependent solution for microstrip transmission lines," *IEEE Trans. Microwave Theory Tech.*, vol. MTT-19, pp. 30–39, Jan. 1971.

[2] T. Itoh and R. Mittra, "Spectral-domain approach for calculating the dispersion characteristics of microstrip lines," *IEEE Trans. Microwave Theory Tech.*, vol. MTT-21, pp. 496–499, July 1973.

[3] E. F. Kuester and D. C. Chang, "An appraisal of methods for computation of the dispersion characteristics of open microstrip," *IEEE Trans. Microwave Theory Tech.*, vol. MTT-27, pp. 691–694, July 1979.

[4] E. Yamashita, K. Atsuki, and T. Ueda, "An approximate dispersion formula of microstrip lines for computer-aided design of microwave integrated circuits," *IEEE Trans. Microwave Theory Tech.*, vol. MTT-27, pp. 1036–1038, Dec. 1979.

[5] M. Hashimoto, "A rigorous solution for dispersive microstrip," *IEEE Trans. Microwave Theory Tech.*, vol. MTT-33, pp. 1131–1137, Nov. 1985.

[6] M. Kobayashi and F. Ando, "Dispersion characteristics of open microstrip lines," *IEEE Trans. Microwave Theory Tech.*, vol. MTT-35, pp. 101–105, Feb. 1987.

[7] E. Yamashita and K. K. Atsuki, "Analysis of microstrip-like transmission lines by nonuniform discretization of integral equations," *IEEE Trans. Microwave Theory Tech.*, vol. MTT-24, pp. 195–200, Apr. 1976.

[8] Y. Fukuoka, Q. Zhang, D. Neikirk, and T. Itoh, "Analysis of multilayer interconnection lines for a high-speed digital integrated circuit," *IEEE Trans. Microwave Theory Tech.*, vol. MTT-33, pp. 527–532, June 1985.

[9] R. H. Jansen, "Unified user-oriented computation of shielded, covered and open planar microwave and millimeter-wave transmission-line characteristics," *Microwaves, Opts., Acoust.*, vol. 3, pp. 14–22, Jan. 1979.

[10] R. H. Jansen, "The spectral domain approach for microwave integrated circuits," *IEEE Trans. Microwave Theory Tech.*, vol. MTT-33, pp. 1043–1056, Oct. 1985.

[11] J. Meixner, "The behavior of electromagnetic fields at edges," *IEEE Trans. Antennas Propagat.*, vol. AP-20, pp. 442–446, July 1972.

[12] L. B. Felsen and N. Marcuvitz, *Radiation and Scattering of Waves*. Englewood Cliffs, NJ: Prentice-Hall, 1973.

[13] M. Abramowitz and I. A. Stegun, *Handbook of Mathematical Functions with Formulas, Graphs, and Mathematical Tables*. New York: Dover, 1964.

✠

Niels Faché was born in Ghent, Belgium, on July 4, 1964. He received a degree in electrical engineering from the University of Ghent in 1986. He is working toward the Ph.D. degree in electrical engineering at the University of Ghent. His research concerns the electromagnetic modeling of microwave interconnections.

✠

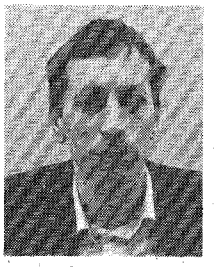

Daniël De Zutter was born in Eeklo, Belgium, on November 8, 1953. He received the degree of electrical engineer from the University of Ghent, Belgium, in 1976. From September 1976 to September 1984 he was a research and teaching assistant at the Laboratory of Electromagnetism and Acoustics (LEA) of the same university. In October 1981 he obtained the Ph.D. degree from that university and in the spring of 1984 he completed a thesis leading to a degree equivalent to the French Aggrégation or the German Habilitation.

Most of his scientific work deals with the electrodynamics of moving media, with emphasis on the Doppler effect and the forces involved in the interaction of fields with moving media. At present he works at the LEA as a Research Associate of the National Fund for Scientific Research of Belgium. His major research topics are hyperthermia, in particular the field calculations inside biological tissues, the electrodynamics of moving media applied to magnetic levitation and suspension, and the propagation characteristics of high-frequency interconnections.